Interdigitated impedimetric-based Maackia amurensis lectin biosensor for prostate cancer biomarker

Siti Fatimah Abd Rahman, Mohd Khairuddin Md Arshad, Subash C B Gopinath, Mohamad Faris Mohamad Fathil, Frédéric Sarry, Conlathan Ibau, Omar Elmazria, Sami Hage-Ali

Interdigitated Impedimetric-based *Maackia amurensis* Lectin Biosensor for Prostate Cancer Biomarker

Siti Fatimah Abd Rahman [1,2], Mohd Khairuddin Md Arshad [1,3,*] , Subash C. B. Gopinath [1,4] , Mohamad Faris Mohamad Fathil [1] , Frédéric Sarry [5] , Conlathan Ibau [1] , Omar Elmazria [5], Sami Hage-Ali [5] and Asrulnizam Abd Manaf [2,6]

[1] **Institute of Nano Electronic Engineering, Universiti Malaysia Perlis, 01000 Kangar, Perlis, Malaysia.**
[2] **School of Electrical and Electronic Engineering, Engineering Campus, Universiti Sains Malaysia, 14300 Nibong Tebal, Pulau Pinang, Malaysia.**
[3] **Faculty of Electronic Engineering and Technology, Universiti Malaysia Perlis, 02600 Arau, Perlis, Malaysia**
[4] **Faculty of Chemical Engineering Technology, Universiti Malysia Perlis, 02600 Arau, Perlis, Malaysia.**
[5] **Université de Lorraine, CNRS, IJL, F-54000 Nancy, France.**
[6] **Collaborative Microelectronic Design Excellence Center, Universiti Sains Malaysia, 11900 Bayan Lepas, Pulau Pinang, Malaysia.**

Correspondence to:

Prof. Ir. Dr. Mohd Khairuddin Md Arshad
Institute of Nano Electronic Engineering,
Universiti Malaysia Perlis,
Lot 106, 108 & 110, Tingkat 1, Block A,
Taman Pertiwi Indah, Jalan Kangar-Alor Setar,
Seriab 01000 Kangar, Perlis, Malaysia
Tel: +604-9798581
Email: mohd.khairuddin@unimap.edu.my

Abstract

Highly specific detection of tumor-associated biomarkers remains a challenge in the diagnosis of prostate cancer (PCa). In this research, *Maackia amurensis* (MAA) was used as a recognition element in the functionalization of an electrochemical impedance-spectroscopy biosensor without a label for the detection of PCa-associated aberrant glycosylation prostate-specific antigen (PSA). The lectin was immobilized on gold-interdigitated microelectrodes. Furthermore, the biosensor's impedance response was used to assess the establishment of a complex binding between MAA and PSA-containing glycans. With a small sample volume, the functionalized interdigitated impedimetric-based (IIB) biosensor exhibited high sensitivity, rapid response, and repeatability. The increase in electron transfer resistance was proportional to PSA glycoprotein concentration in a range of 100 ng/mL to 10 pg/mL, with a detection limit of 3.574 pg/mL. In this study, the ability of MAA to preferentially recognize α2,3-linked sialic acid in serum PSA was proven, suggesting a potential platform for the development of lectin-based, miniaturized, and cost effective IIB biosensors for future disease detection.

Keywords: impedimetric biosensor; lectin; glycosylation; prostate-specific antigen; biomarkers; prostate cancer.

1. Introduction

Technology enabled the detection of disease biomarkers with high accuracy, and affordability at point-of-care locations is currently one of the main challenges in the biosensor research field. Ideally, the use of biomarkers for cancer diagnosis is of great significance to identify at-risk men as early as possible and, therefore, reduce the number of cancer-related deaths. Moreover, detecting cancer biomarkers in biological fluids, such as blood, is thought to be the best way to create non-invasive screening assays (Díaz-Fernández et al., 2020; Kirwan et al., 2015).

Prostate cancer (PCa) is the leading cause of cancer death in men worldwide, with a 55% mortality rate recorded in less developed regions, including Africa, Asia, and Latin America (Rawla, 2019). Prostate-specific antigen (PSA), a glycoprotein produced by the prostate, is the most commonly used cancer biomarker. Since the early 1990s, screening for PSA levels in blood serum has been the gold standard for diagnosing possible cancerous abnormalities of the prostate. In men, the PSA level should be less than 4 ng/mL (cut-off point); otherwise, PCa should be suspected, and further investigation via biopsy is required (Drake et al., 2015; Kirwan et al., 2015). However, the efficacy of current approaches is controversial since numerous

factors, including prostatitis, irritation, and benign prostatic hyperplasia (BPH), can elevate the serum PSA level. This leads to overdiagnosis and overtreatment due to the false-positive results of PSA-based PCa screening (Gilgunn et al., 2013; Lilja et al., 2008). Therefore, finding novel biomarkers with improved specificity is of vital importance.

Recent advances in glycomics have shed light on the diagnostic role of aberrant glycosylation in oncological diseases, and it has been described as a hallmark of cancer. Glycosylation is an important post-translational modification event in the human body that involves the covalent attachment of carbohydrate moieties to proteins; it occurs in about half of all serum proteins. Therefore, early detection of these altered glycoproteins with tumor-specific glycan moieties may improve treatment outcomes (Belick and Katrl, 2016; Belický and Tkac, 2014; Scott and Munkley, 2019). There is enough evidence in the literature highlighting the critical roles of sialic acids in cancer initiation, progression, and immune evasion of the host (Pearce and Läubli, 2015), including breast (Hernández-Arteaga et al., 2019), ovarian (Berghuis et al., 2022), lung (Elgohary et al., 2018), and prostate cancers (Pihikova et al., 2016b). Sialic acids are nine carbon alpha-keto acid sugars attached at the termini of glycoprotein carbohydrate chains. *N*–acetylneuraminic acid (Neu5Ac) is the most prevalent sialic acid in humans. Approximately 80% of Neu5Ac-conjugated glycans are found in glycoproteins, including PSA. PSA has a single *N*–glycosylation site attached to the amine nitrogen of asparagine 69 (Asn-69) (Büll et al., 2014; Kałuża et al., 2021). Note that the linking site in the glycan composition of PSA changes during carcinogenesis (Gilgunn et al., 2013); in keeping with this fact, the sialylation of PSA N–glycans have been extensively studied. In accordance, Belicky et al. (Belicky et al., 2017) described a significant increase in α2,3-linked sialic acid in PCa patients (Gleason scores: 5 and 7) compared with patients with BPH. These observations are consistent with the findings of Ohyama et al. (Ohyama et al., 2004), who reported an increase in α2,3-linked sialic acid in serum PSA from prostate cancer patients compared with BPH. Furthermore, Silva et al. (Silva et al., 2016) discovered that the α2,3-linked sialic acid was upregulated in prostate tumors, whereas healthy individuals expressed predominant levels of α2,6-sialylated PSA. This indicates that determining specific glycans, such as α2,3-linked sialic acid in glycosylated PSA, could be a valuable biomarker for improving the specificity of prostate cancer diagnoses.

Conventionally, analysis of glycoprotein glycans has been represented by mass spectrometry in conjunction with high-performance liquid chromatography or capillary electrophoresis (Alley et al., 2013; Vermassen et al., 2012). These approaches have high sensitivity and reproducibility, but they require prior liberation of the attached glycans from

their core proteins and are usually fluorescently labelled. For these reasons, the advanced spectrometric methods are time-consuming, extremely sophisticated, and costly, requiring highly skilled operators. Significantly, a series of promising methods for glycan analyses based on lectin-binding capacity, e.g., enzyme-linked immunosorbent assay (ELISA) and microarray-based technology, have been introduced (Hirabayashi et al., 2013; Shimomura et al., 2015). In general, lectins are natural proteins with carbohydrate-binding sites that can specifically bind both free glycans and glycans attached to glycoconjugates (Lam and Ng, 2011), such as PSA glycoproteins. Although both methods provide a useful approach for lectin-based diagnostic applications, low sensitivity of assays, narrow detection range, and the need to apply labels are the main drawbacks that need to be addressed.

In this sense, Rahman et al. (Rahman et al., 2021) proposed a key consideration regarding the efficiency of biosensor technology in a recent review, which discusses in depth the concept, strategy, and technical advancement of glycosylated biomarker sensors. The electrochemical detection method, specifically the electrochemical impedance spectroscopy (EIS)-based sensing, was reported as a strategy well-suited for lectin–glycan analysis for PCa diagnosis in a label-free fashion. Phikova et al. (Pihikova et al., 2016a) developed an immunosensor-based screen-printed electrode (SPE) to detect PSA glycans using *Maackia amurensis* lectin in a sandwich format. The impedimetric assessment was employed, and the sensor recorded a detection limit down to 100 ag/mL. Esther et al. (Sánchez-tirado et al., 2018) developed another lectin-SPE immunosensor in combination with magnetic multi-walled carbon nanotubes for impedimetric detection of PCa glycoprotein. A detection limit of 16 pg/mL was achieved. Despite the well-established SPE and EIS-based electrochemical platform advantage, the use of interdigitated electrode (IDE) as a sensing transducer for PCa detection is not yet well explored in the literature.

IDE consists of two interlocking interdigitated fingers, with each section having a series of parallel comb-like electrode structures connected and separated by insulators. In the electrical aspect, IDE is an interesting device architecture, with a small amplitude sinusoidal excitation signal. The high sensitivity levels required for many applications can be achieved using low-cost IDE with submicron electrode width and gap dimensions, thus eliminating the need for expensive conventional macro-electrode technologies. Furthermore, the use of interdigitated electrode arrays is not limited to capacitive and resistive sensors but can also be extended to impedimetric sensors (Dalila R et al., 2022). Notably, most early reports focused on basic fabrication procedures of IDE due to their ease of miniaturization, batch fabrication, and automation (Kuphal et al., 2012; Tang et al., 2011), while recent publications are

increasingly concerned about applications of this technology as a low-cost point-of-care (POC) diagnostic with operation simplicity, reliability, and portability (Sharma et al., 2022; Supraja et al., 2021).

Inspired by these shining points, we designed a lectin-based interdigitated impedimetric-based (IIB) biosensor as a sensing platform for detecting PSA glycoprotein in PCa application. *Maackia amurensis* (MAA), a lectin with an affinity toward α2,3-linked sialic acid, is used as a molecular recognition element for highly specific detection of glycosylated PSA biomarkers. The proposed IIB biosensor possesses numerous advantages, such as high sensitivity and selectivity, low volume sample, reusability, repeatability, and low detection limit. The sensor is also efficient detecting cancer biomarkers in serum at the picomolar level. Furthermore, a simple method that functions effectively without complex equipment or user expertise is introduced. All these advantages make the IIB biosensor impeccable for label-free testing of PCa in its early stages.

2. Material and methods

2.1. Assay procedures and apparatus

To investigate the charge transfer resistance (Rct), electrochemical impedance spectroscopy measurements were performed using a dielectric analyzer (Novocontrol Technologies, Germany). The cyclic voltametric (CV) variations were analyzed using an electrochemical potentiostat PGSTAT 204 (Metrohm Autolab) and the Nova Software 1.10 (Ecochemie, The Netherlands). DropSens (Metrohm Malaysia Sd. Bhd.) provided interdigitated microelectrodes (IDE, DRP-G-IDE222), which were utilized in all experiments. The device consists of IDE as working electrodes, an auxiliary electrode, and a reference electrode, all of which were fabricated on a glass substrate using gold (Au). The EIS measurements were recorded at frequencies of 0.1−100 kHz while a 200-mV alternating current voltage was applied in a newly produced electrolyte comprising 5 mM potassium hexacyanoferrate (III), 5 mM potassium hexacyanoferrate (II), and 10 mM phosphate-buffered saline (PBS) pH 7.4. The output signal was the change in Rct compared to the reference surface (e.g., biosensor surface after lectin immobilization). All experiments were performed at room temperature.

2.2. IDE sensing surface modifications

Electrodes were carefully cleaned using acetone, isopropanol, and deionized water (DIW), accompanied by air drying. The gold electrode surface was utilized in threating 11-mercaptoundecanoic acid (MUA) to form a congregated monolayer. The technique was derived from previous reported work (Ibau et al., 2020) with minor adjustments. Thus, 30 µL of 5 mM 11-MUA was maintained at a particular temperature for 12 hours at 4°C on the detecting surface before being rinsed with PBS pH 7.4. The combined N-hydroxysuccinimide (EDC) / 1-ethyl-3-(3-(dimethylamino) propyl) carbodiimide (NHS) solution (4:1) was then maintained at a particular temperature for 60 minutes at 4°C on the altered sensor surface. This step was applied to initiate the carboxyl-terminated 11-MUA on the gold surface electrode in preparation for additional lectin immobilization.

Prior to application, MAA lectin (Fisher Scientific, UK) was diluted in PBS with a pH value of 7.4 to reach a concentration of 1.0 µg/mL. During the immobilization procedure, the prepared MAA lectin was incubated for 1 hour at 4°C on the altered sensing surface and washed with PBS. The electrode was then incubated in 200 mM ethanolamine for 1 hour at 4°C before being washed with PBS. Nonspecific binding was inhibited by the application of this blocking agent. The target PSA glycosylation (SinoBiological, Beijing, China) was utilized to incubate the modified electrode for 1 hour at 4°C. Different target concentrations ranging from 10 pg/mL to 100 ng/mL was employed with amounts of 20 µL for every detection phase. Working detection was carried out from the lowest to highest target concentrations. Fig. 1 depicts the lectin–PSA sensing using IIB biosensor.

Figure 1

2.3. Surface characterization and binding analysis

Scanning electron microscopy (SEM) in combination with energy-dispersive X-ray spectroscopy (EDS) (JSM-6010LV JEOL, Japan) with a resolution range of 4 nm was used to characterize the gold interdigitated electrodes. A profiler surface analysis (WT-250 Series, Hawk 3D Nano-Profiler, Korea) was used for surface topography analysis. This non-destructive optical measurement system is attached with HAWK 3D Surface Analysis to measure the three-dimensional (3D) vision of the electrodes. X-ray photoelectron spectroscopy (XSAM-H, Kratos, UK) was used to characterize the elemental composition and chemical state of the samples. An atomic force microscope (AFM) in ambient tapping mode (SPA400 Seiko Instrument Inc., Japan) and a VCA 300 water surface analysis system (AST Products, Inc.,

Billerica, MA) were conducted to characterize the consecutively prepared samples, i.e., bare and EDC/NHS functionalized, respectively. To study the hydrophobicity and hydrophilicity of the electrode surface, a constant drop of DIW with size 6.50 µL was dispensed to each samples surface (horizontal position) on a motorized stage by means of a motorized syringe. Subsequently, the images of the droplet were captured using a high-resolution VCA 3000S's camera. VCA Optima software was used to determine tangent lines for the basis of contact angle measurements. Furthermore, the gold standard method, ELISA, was performed to justify the impedimetric results obtained using the developed biosensor for lectin and target protein specific binding.

3. Results and discussion

3.1. Electrode surface characterization

Surface morphologies of the bare gold-interdigitated microelectrode was characterized using SEM/EDS. Fig. 2A shows the device topology as imaged at magnifications of x35 and electron energy of 15 kV. It can be observed that the device comprised two weaved comb-like electrodes which emerge from wide busbars. Each finger of the electrodes is approximately 10 µm width and interdigitated gaps at 9 µm. The active sensing area which was covered by the fingers is about 3.4 mm × 3.4 mm. The EDS characterization data reveals the elemental composition of the gold (Au) in the electrodes.

Then, the surface topography was observed using a 3D-nanoprofiler as presented in Fig. 2B. The glass substrate and Au finger electrode surface can be seen significantly by the color variation of each layer. The blue color indicates the glass surface while the yellow-orange color indicates the Au interdigitated electrode. The average height of the electrode from the base level is approximately 71.2 µm, with the uniform length and gap of each finger's electrodes. The surface modification effects of thiolation chemistry on the Au electrode surface were topographically studied using contact angle measurements and an atomic force microscope.

Figure 2

Fig. 3A shows the AFM-based characterization results for the bare and modified electrode surfaces. Our investigations revealed that the surface exhibited differing morphologies and heights at the microscale level. Specifically, while the cleaned gold surface had a homogeneous morphology [Fig. 3A (i)], an increase in height and significant changes in

surface roughness were observed after chemical modifications using EDC/NHS on the self-assembled Au-electrode surface monolayer [Fig. 3A (ii)], including a decrease in the mean surface roughness (Ra) and maximum roughness (Rmax) from 1.23 and 9.37 to 0.98 and 5.66, respectively, confirming the successful modification of 11-MUA/EDC/NHS on the electrode's surface.

Notably, the roughness of a surface is significant because it plays a crucial role in inducing wettability. Therefore, surface wettability is another physicochemical parameter to estimate the hydrophilicity or hydrophobicity of a material's surface, commonly characterized by the contact angle formed by a liquid droplet. For example, the shape of a liquid droplet deposited on a solid substrate can form a three-phase contact line when the liquid is in contact with both a vapor phase and a solid phase (West, 2018). In such cases, the contact angle values that reflect the surface's chemical and physical constitutions: functional groups, chemical modifications, or topological features can be determined based on the tangent of the liquid–vapor contact line making an angle *(θ)* with the horizontal surface (Ubuo et al., 2021; West, 2018). Hence, considering these parameters, the patterns at which such wetting occurs have been represented by the Wenzel and Cassie–Baxter models, i.e., the homogeneous composite wetting state and the heterogeneous composite wetting state (Swain and Lipowsky, 1998; West, 2018), respectively.

In this regard, the water contact angle measurements were conducted to further validate the Au-electrode surface's chemical modifications. Fig. 3B shows an initial contact angle of 44° ± 2° for the cleaned gold surface, reflecting the Wenzel state. This hydrophilic film behavior can be explained by the fact that since the water was in contact with a homogeneous surface of same composition (Ubuo et al., 2021; West, 2018), it filled the rough surface, forming a fully wet contact. Conversely, adding an 11-MUA/EDC/NHS layer made the surface hydrophobic by increasing the contact angle to 61° ± 2°. Hence, we propose that the hydrophobicity of the surface increased due to the formation of a succinimide ester (Yan et al., 2015), which is efficiently used to covalently couple amine-containing biomolecules *via* amide linkages, comparable with previous works (Lim et al., 2014; Nam et al., 2008), suggesting that the crosslinking method using EDC/NHS can induce the formation of an amide bond by activating carboxylic acid groups. Investigation also revealed that the chemical modification process induces a rougher surface that substantially alters the material's wettability (Ubuo et al., 2021). However, the results do not comply with the Wenzel equation, which states that any increase in the Wenzel roughness should serve to decrease the contact angle when θ is less than 90° (Zeng, 2018). This mode of wetting is, thus, analogous to the one based on the Cassie–

Baxter model, which involves chemical and physical surface heterogeneities (West, 2018), i.e., the surface coverage of the ester and carboxylic moieties.

Figure 3

X-ray photoelectron spectroscopy (XPS) analysis was performed to gain an in-depth understanding of the elemental composition of the surface functionalization results. Fig. 4A–D, respectively, display the high-resolution spectra scans for the XPS bands C 1s, O 1s, N 1s, and S 2p for carbon, oxygen, nitrogen, and sulfur atoms. Characterization was performed on bare Au, and then the results were compared with the sample obtained by the activation of the self-assembled monolayer (SAM) of 11-MUA on the Au surface using EDC/NHS. The XPS profile of the bare Au surface shows C 1s (Fig. 4A) and O 1s (Fig. 4B) peaks, as a result of hydrocarbon (C–H) impurities and the formation of hydroxyl (–OH) species during the cleaning process, respectively. Indeed, all binding energies (BEs) were referenced to the C 1s peak observed at 284.8 eV for bare Au.

Figure 4

In the high-resolution C 1s profile obtained after the activation of 11-MUA with EDC/NHS (Fig. 4A), core peaks appeared at 286.5 and 289.0 eV, indicating the presence of C–CON and –COOH bonds of the NHS ester (Ko and Ma, 2009), respectively. This observation qualitatively clarifies that the carboxyl groups were involved in cross-linking, and supports the hypothesis made based on the measured contact angle. Whilst the peak at 286.1 eV was assigned to carbon-bound sulfur (C–S) (Mendoza et al., 2007), the O 1s spectra for the sample activated using EDC/NHS showed two peaks attributable to amide/carbonyl (N–C=O/C=O) and C–O–N components of the NHS ester at BE values of 533.7 and 534.4 eV (Delamarche et al., 1996), respectively (Fig. 4B). Another validation of the amide peak was obtained from the peak at the BE of 402.3 eV in the N 1s spectrum of functionalized Au (Böcking et al., 2006) (Fig. 4C). The sharp peak at 400 eV corresponds to the tertiary amines group ($–NH_3^+$) (Niedermaier et al., 2012). Furthermore, the signal at 161.9 eV (Fig. 4D) can be assigned to Au-bonded sulfur atoms (Au–S) owing to SAM formation, whereas the component at 163.7 eV is characteristic of unbound thiol groups (–SH) or weakly interacting sulfur atoms (Castner et al., 1996). Another peak appeared at 168 eV, indicating that the SAM

thiol group had oxidized. This shows that 11-MUA/EDC/NHS successfully bonded to the Au surface, which was not observed before the functionalization.

3.2. Analytical performance of the IIB biosensor

The electrocatalytic response of each modified step was monitored using the CV technique in the presence of 10 mM potassium ferrocyanide and 10 mM potassium chloride to characterize the behavior of the fabricated biosensor. Ferrocyanide ion $[Fe(CN)_6]^{3-/4-}$ has been used as an effective redox probe for examining the redox properties toward the electrode surface because of its reversibility and rapid electrochemical reactions (Azmi et al., 2018). As illustrated in Fig. 5A, a well-defined redox peak of $[Fe(CN)_6]^{3-/4-}$ was obtained at the bare gold interdigitated electrode. The peak current was successively reduced to 110 nA following the surface modification processes utilizing 11-MUA/EDC/NHS. These reductions are attributed to resistive layer formation on the modified surface electrode, which led to a reduction in peak oxidation currents. With incubation of the MAA lectin and after the blocking with ethanolamine to the nonspecific sites of the electrode, the peak current decreased obviously to 43 nA. This is primarily due to the possibility that protein biomolecules could prevent the redox probe's ability to transfer electrons. These findings supported the EIS finding, indicating that the proposed IIB biosensor was created successfully.

The EIS method was used for interfacial investigation of the stepwise modification process by using the interdigitated microelectrodes as detectors. Measurements of the variations in charge transfer resistance (Rct) and total impedance (Z) versus frequency as a result of the lectin-glycan PSA binding were used to develop a detection strategy. The change in the Rct values corresponded to the charge transfer process between the $[Fe(CN)_6]^{3-/4-}$ redox species and the modified interfacial layer on the electrode surface (Fig. 5B). Depending on the electrode voltage, a faradaic current is produced by the species' charge transfer. As a result, the interfacial impedance was sensitive to the presence of compounds that were immobilized or adsorbed.

Figure 5

The physical blocking effects of the proteins binding complex interfere with the kinetics of the redox reagent close to the electrodes when lectin-glycan binding takes place. This phenomenon suppresses the charge transfer process by the redox reaction of the reagent. The IIB biosensor's changed impedance is primarily responsible for the reduced charge transfer (or

equivalently increased Rct). To calculate the concentration of the target molecules, the change in Rct is quantitatively monitored. As more glycan reacts with immobilized lectin, the physical blocking effect of the lectin-glycan binding complex further increases, and therefore results in a very specific and highly sensitive magnitude of the Rct values.

The electrochemical data was fitted using Randles equivalent circuit shown in the inset of Fig. 5C. The circuit includes of the resistance of electrolyte solution (Rs) in series with the parallel of a constant phase element (Q) and the Warburg impedance (Zw) that was in series combination with the measured Rct. As seen in Fig. 5C, successful immobilization is indicated by a rise in Rct from 0.4 MΩ for the unaltered device to 0.7 MΩ following lectin and ethanolamine-blocking creation. This is because the impedance considerably increased after the lectin was attached since the development of the probe's monolayer prevented current flow. These findings corroborate the results of the CVs and were well reflected in the Rct. After that, the lectin-glycan PSA binding on the Au electrode surface was investigated using the MAA-based IIB in the 10 pg/mL to 100 ng/mL concentration range. The increasing Rct values were obtained for increasing PSA proteins onto the surface-bound lectin. The varying lectin-glycan conformation is responsible for this change in Faradaic-based impedimetric measurement.

The sensitivity measurement of the developed IIB biosensor is verified using the impedance vs. concentration relation given by the linear regression equation of the plots is $y = 1.47 \log_{10} x + 0.41$. This can be express as $y = m \log_{10} x + c$, where m is the slope and c is the y-intercept of the line. Thus, the corresponding y-intercept value resulted from linear regression on the logarithms is found to be 0.41. For the logarithmic x-axis (concentration in ng/mL), the y-intercept is the point where the graph of the function crosses the y-axis when $\log_{10} x$ equals 0. Given the $\log_{10} 1$ is 0, therefore the value of y where the line crosses the x = 1 axis gives us the y-intercept. This prove that the y-intercept is 0.41 when the x-axis is 10^0 ($\log_{10} 1 = 0$) as shown in inset of Fig. 5D. The error bars in Fig. 5D illustrate that every measurement was carried out three times, and different electrodes were found to give similar responses within 5% of each other. The sensor showed a sensitivity of 1.47 MΩ/$\log_{10}$ [PSA] (ng/mL) with a correlation coefficient of 0.9918 demonstrating the reliability of the biosensor. In addition, the limit of detection (LOD) was estimated based on the equation of LOD = 3 σ, where σ is the standard deviation of the linear coefficient. The LOD value for the IIB biosensor was 3.574 pg/mL, which is lower than the established clinical cut-off value (4 ng/mL) for serum PSA in PCa patients.

3.3. Detection specificity in undiluted human serum

The immobilized MMA electrodes were incubated with a non-PSA biomarker as shown in Fig. 6A in order to evaluate and validate the specificity of the biosensor response. The results showed that there was no significant change in impedance, which demonstrates the absence of unspecific adsorptions even on the surface electrode. Furthermore, the feasibility of the developed sensors for clinical applications was tested in an undiluted human serum (HS) spiked with glycosylated PSA concentrations of 1 ng/mL and 10 ng/mL. The setup evaluated the interaction between surface bound MAA lectin and α2,3-linked sialic acid in glycosylated PSA while discriminating other inherent proteins in the serum, which demonstrates the high specificity of the sensors. In addition, a gold standard ELISA analysis was performed in validating the results obtained by the IIB biosensor (Fig. 6B). The optical results revealed that color change from a clear solution to a blue solution occurred for the wells containing undiluted HS spiked with glycosylated PSA in the concentrations of 1 ng/mL and 10 ng/mL, while no color changes were observed for the undiluted HS samples.

Figure 6

The results show the significant potential of the IIB biosensor in the direct assessment of undiluted HS, thus enabling reliable quantitative analyses of real serum samples with high sensitivity as compared with the standard ELISA technique. Furthermore, this simple impedimetric method functions efficiently without signal amplification and response within an hour in a single incubation step. Therefore, the IIB biosensor developed in this study is suitable for early and specific PCa detection.

4. Conclusion

Sialylated glycoproteins are a rapidly expanding field of study that probably play crucial roles in the development of PCa. This study presented a simple fabrication method of MAA-based interdigitated impedimetric biosensor for sensitive and specific detection of α2,3-linked sialic acid PCa biomarkers. The biosensor displayed high selectivity, a broad detection range of 10 pg/mL to 100 ng/mL, and high sensitivity of 1.47 MΩ/$\log_{10}$ [PSA] (ng/mL) in a label-free manner. The detection limits can reach as low as 3.574 pg/mL (LOD = 3 σ) within an hour from 20 µL of target samples. The IIB biosensors are more user-friendly and capable of testing undiluted human serum spiked with glycosylated PSA directly than the traditional ELISA method, which opens up a wider range of potential applications for point-of-care PCa biomarkers detection in clinical settings. Future biofluids of PCa patients, specifically serum samples from hospitals, will be organized with great effort.

Acknowledgements

This work was supported by the Ministry of Education Malaysia through the (MyPAIR) Hubert Curien Partnership – Hibiscus Grant, grant number MyPAIR/1/2020/STG05/UniMAP/1.

References

Alley, W.R., Mann, B.F., Novotny, M.V., 2013. High-sensitivity analytical approaches for the structural characterization of glycoproteins. Chem. Rev. 113, 2668–2732.

Azmi, U.Z.M., Yusof, N.A., Kusnin, N., Abdullah, J., Suraiya, S., Ong, P.S., Raston, N.H.A., Rahman, S.F.A., Fathil, M.F.M., 2018. Sandwich electrochemical immunosensor for early detection of tuberculosis based on graphene/polyaniline-modified screen-printed gold electrode. Sensors (Switzerland) 18, 1–14. https://doi.org/10.3390/s18113926

Belick, S., Katrl, J., 2016. Glycan and lectin biosensors ˇ. Essays Biochem. 60, 37–47. https://doi.org/10.1042/EBC20150005

Belicky, S., Černocká, H., Bertok, T., Holazova, A., Réblová, K., Paleček, E., Tkac, J., Ostatná, V., 2017. Label-free chronopotentiometric glycoprofiling of prostate specific antigen using sialic acid recognizing lectins. Bioelectrochemistry 117, 89–94. https://doi.org/10.1016/j.bioelechem.2017.06.005

Belický, Š., Tkac, J., 2014. Can glycoprofiling be helpful in detecting prostate cancer? Chem. Pap. 69, 90–111. https://doi.org/10.1515/chempap-2015-0052.Can

Berghuis, A.Y., Pijnenborg, J.F.A., Boltje, T.J., Pijnenborg, J.M.A., 2022. Sialic acids in gynecological cancer development and progression: Impact on diagnosis and treatment. Int. J. Cancer 150, 678–687. https://doi.org/10.1002/ijc.33866

Böcking, T., Wong, E.L.S., James, M., Watson, J.A., Brown, C.L., Chilcott, T.C., Barrow, K.D., Coster, H.G.L., 2006. Immobilization of dendrimers on Si–C linked carboxylic acid-terminated monolayers on silicon(111). Thin Solid Films 515, 1857–1863. https://doi.org/10.1016/j.tsf.2006.07.017.

Büll, C., Stoel, M.A., Den Brok, M.H., Adema, G.J., 2014. Sialic acids sweeten a tumor's life. Cancer Res. 74, 3199–3204. https://doi.org/10.1158/0008-5472.CAN-14-0728

Castner, D.G., Hinds, K., Grainger, D.W., 1996. X-ray Photoelectron Spectroscopy Sulfur 2p Study of Organic Thiol and Disulfide Binding Interactions with Gold Surfaces. Langmuir 12, 5083–5086. https://doi.org/10.1021/la960465w

Dalila R, N., Arshad, M.K.M., Gopinath, S.C.B., Ibau, C., Nuzaihan M. N. , M., Fathil, M.F.M., Azmi, U.Z.M., Anbu, P., 2022. Faradaic electrochemical impedimetric analysis on MoS2/Au-NPs decorated surface for C-reactive protein detection. J. Taiwan Inst. Chem. Eng. 138. https://doi.org/10.1016/j.jtice.2022.104450

Delamarche, E., Sundarababu, G., Biebuyck, H., Michel, B., Gerber, C., Sigrist, H., Wolf, H., Ringsdorf, H., Xanthopoulos, N., Mathieu, H.J., 1996. Immobilization of Antibodies on a Photoactive Self-Assembled Monolayer on Gold. Langmuir 12, 1997–2006. https://doi.org/10.1021/la950836t

Díaz-Fernández, A., Lorenzo-Gómez, R., Miranda-Castro, R., de-los-Santos-Álvarez, N., Lobo-Castañón, M.J., 2020. Electrochemical aptasensors for cancer diagnosis in biological fluids – A review. Anal. Chim. Acta 1124, 1–19. https://doi.org/10.1016/j.aca.2020.04.022

Drake, R.R., Jones, E.E., Powers, T.W., Nyalwidhe, J.O., 2015. Altered glycosylation in prostate cancer, 1st ed, Advances in Cancer Research. Elsevier Inc. https://doi.org/10.1016/bs.acr.2014.12.001

Elgohary, M.M., Helmy, M.W., Abdelfattah, E.Z.A., Ragab, D.M., Mortada, S.M., Fang, J.Y., Elzoghby, A.O., 2018. Targeting sialic acid residues on lung cancer cells by inhalable boronic acid-decorated albumin nanocomposites for combined chemo/herbal therapy. J. Control. Release 285, 230–243. https://doi.org/10.1016/j.jconrel.2018.07.014

Gilgunn, S., Conroy, P.J., Saldova, R., Rudd, P.M., O'Kennedy, R.J., 2013. Aberrant PSA glycosylation - A sweet predictor of prostate cancer. Nat. Rev. Urol. 10, 99–107.

Hernández-Arteaga, A.C., de Jesús Zermeño-Nava, J., Martínez-Martínez, M.U., Hernández-Cedillo, A., Ojeda-Galván, H.J., José-Yacamán, M., Navarro-Contreras, H.R., 2019. Determination of Salivary Sialic Acid Through Nanotechnology: A Useful Biomarker for the Screening of Breast Cancer. Arch. Med. Res. 50, 105–110. https://doi.org/10.1016/j.arcmed.2019.05.013

Hirabayashi, J., Yamada, M., Kuno, A., Tateno, H., 2013. Lectin microarrays: Concept, principle and applications. Chem. Soc. Rev. 42, 4443–4458. https://doi.org/10.1039/c3cs35419a

Ibau, C., Arshad, M.K.M., Gopinath, S.C.B., Nuzaihan, M., Fathil, M.F.M., Shamsuddin, S.A., 2020. Immunosensing prostate-specific antigen: Faradaic vs non-Faradaic electrochemical impedance spectroscopy analysis on interdigitated microelectrode device. Int. J. Biol. Macromol. 162, 1924–1936. https://doi.org/10.1016/j.ijbiomac.2020.08.125

Kałuża, A., Szczykutowicz, J., Ferens-Sieczkowska, M., 2021. Glycosylation: Rising potential for prostate cancer evaluation. Cancers (Basel). 13. https://doi.org/10.3390/cancers13153726

Kirwan, A., Utratna, M., O'Dwyer, M.E., Joshi, L., Kilcoyne, M., 2015. Glycosylation-Based Serum Biomarkers for Cancer Diagnostics and Prognostics. Biomed Res. Int. 2015. https://doi.org/10.1155/2015/490531

Ko, Y.G., Ma, P.X., 2009. Surface-grafting of phosphates onto a polymer for potential biomimetic functionalization of biomaterials. J. Colloid Interface Sci. 330, 77–83. https://doi.org/10.1016/j.jcis.2008.10.015

Kuphal, M., Mills, C.A., Korri-Youssoufi, H., Samitier, J., 2012. Polymer-based technology platform for robust electrochemical sensing using gold microelectrodes. Sensors Actuators, B Chem. 161, 279–284. https://doi.org/10.1016/j.snb.2011.10.032

Lam, S.K., Ng, T.B., 2011. Lectins: Production and practical applications. Appl Microbiol Biotechnol 89, 45–55.

Lilja, H., Ulmert, D., Vickers, A.J., 2008. Prostate-specific antigen and prostate cancer: prediction, detection and monitoring. Nat Rev Cancer 8, 268–278.

Lim, C.Y., Owens, N.A., Wampler, R.D., Ying, Y., Granger, J.H., Porter, M.D., Takahashi, M., Shimazu, K., 2014. Succinimidyl Ester Surface Chemistry: Implications of the Competition between Aminolysis and Hydrolysis on Covalent Protein Immobilization. Langmuir 30, 12868–12878. https://doi.org/10.1021/la503439g

Mendoza, S.M., Arfaoui, I., Zanarini, S., Paolucci, F., Rudolf, P., 2007. Improvements in the Characterization of the Crystalline Structure of Acid-Terminated Alkanethiol Self-Assembled Monolayers on Au(111). Langmuir 23, 582–588. https://doi.org/10.1021/la0605539

Nam, K., Kimura, T., Kishida, A., 2008. Controlling coupling reaction of EDC and NHS for preparation of collagen gels using ethanol/water co-solvents. Macromol. Biosci. 8, 32–37. https://doi.org/10.1002/mabi.200700206

Niedermaier, I., Kolbeck, C., Taccardi, N., Schulz, P.S., Li, J., Drewello, T., Wasserscheid, P., Steinrück, H.-P., Maier, F., 2012. Organic Reactions in Ionic Liquids Studied by in Situ XPS. ChemPhysChem 13, 1725–1735. https://doi.org/10.1002/cphc.201100965

Ohyama, C., Hosono, M., Nitta, K., Oh-eda, M., Yoshikawa, K., Habuchi, T., Arai, Y., Fukuda, M., 2004. Carbohydrate structure and differential binding of prostate specific antigen to Maackia amurensis lectin between prostate cancer and benign prostate hypertrophy. Glycobiology 14, 671–9.

Pearce, O.M.T., Läubli, H., 2015. Sialic acids in cancer biology and immunity. Glycobiology 26, 111–128. https://doi.org/10.1093/glycob/cwv097

Pihikova, D., Kasak, P., Kubanikova, P., Sokol, R., Tkac, J., 2016a. Aberrant sialylation of a prostate-specific antigen: Electrochemical label-free glycoprofiling in prostate cancer serum samples. Anal. Chim. Acta 934, 72–9. https://doi.org/10.1016/j.aca.2016.06.043

Pihikova, D., Pakanova, Z., Nemcovic, M., Barath, P., Belicky, S., 2016b. Sweet characterisation of prostate specific antigen using electrochemical lectin-based immunosensor assay and MALDI TOF/TOF analysis : Focus on sialic acid. Proteomics 16, 3085–3095. https://doi.org/10.1002/pmic.201500463

Rahman, S.F.A., Md Arshad, M.K., Gopinath, S.C.B., Fathil, M.F.M., Sarry, F., Ibau, C., 2021. Glycosylated biomarker sensors: advancements in prostate cancer diagnosis. Chem. Commun. 57, 9640–9655. https://doi.org/10.1039/d1cc03080a

Rawla, P., 2019. Epidemiology of Prostate Cancer. World J Oncol 10, 63–89.

Sánchez-tirado, E., González-cortés, A., Yáñez-sedeño, P., Pingarrón, J.M., 2018. Magnetic multiwalled carbon nanotubes as nanocarrier tags for sensitive determination of fetuin in saliva. Biosens. Bioelectron. 113, 88–94. https://doi.org/10.1016/j.bios.2018.04.056

Scott, E., Munkley, J., 2019. Glycans as biomarkers in prostate cancer. Int. J. Mol. Sci. 20, 1389.

Sharma, P.K., Kim, E.S., Mishra, S., Ganbold, E., Seong, R.S., Kim, Y.M., Jahng, G.H., Rhee, H.Y., Han, H.S., Kim, D.H., Kim, S.T., Kim, N.Y., 2022. Ultrasensitive probeless capacitive biosensor for amyloid beta (Aβ1-42) detection in human plasma using interdigitated electrodes. Biosens. Bioelectron. 212, 114365. https://doi.org/10.1016/j.bios.2022.114365

Shimomura, M., Nakayama, K., Azuma, K., Terao, N., Nishino, K., Takamatsu, S., Nakano, M., Takahashi, S., Kobayashi, Y., Murata, K., Kamada, Y., Miyoshi, E., 2015. Establishment of a novel lectin-antibody ELISA system to determine core-fucosylated haptoglobin. Clin. Chim. Acta 446, 30–36. https://doi.org/10.1016/j.cca.2015.03.037

Silva, P.M.S., Lima, A.L.R., Silva, B.V.M., Coelho, L.C.B.B., Dutra, R.F., Correia, M.T.S., 2016. Cratylia mollis lectin nanoelectrode for differential diagnostic of prostate cancer and benign prostatic hyperplasia based on label-free detection. Biosens. Bioelectron. 85, 171–177. https://doi.org/10.1016/j.bios.2016.05.004

Supraja, P., Tripathy, S., Singh, R., Singh, V., Chaudhury, G., Singh, S.G., 2021. Towards point-of-care diagnosis of Alzheimer's disease: Multi-analyte based portable

chemiresistive platform for simultaneous detection of β-amyloid (1–40) and (1–42) in plasma. Biosens. Bioelectron. 186, 113294. https://doi.org/10.1016/j.bios.2021.113294

Swain, P.S., Lipowsky, R., 1998. Contact Angles on Heterogeneous Surfaces : A New Look at Cassie's and Wenzel's Laws. Langmuir 14, 6772–6780. https://doi.org/10.1021/la980602k

Tang, X., Flandre, D., Raskin, J.P., Nizet, Y., Moreno-Hagelsieb, L., Pampin, R., Francis, L.A., 2011. A new interdigitated array microelectrode-oxide-silicon sensor with label-free, high sensitivity and specificity for fast bacteria detection. Sensors Actuators, B Chem. 156, 578–587. https://doi.org/10.1016/j.snb.2011.02.002

Ubuo, E.E., Udoetok, I.A., Tyowua, A.T., Ekwere, I.O., Al-shehri, H.S., 2021. The Direct Cause of Amplified Wettability : Roughness or Surface Chemistry ? J. Compos. Sci. 5, 1–9.

Vermassen, T., Speeckaert, M.M., Lumen, N., Rottey, S., Delanghe, J.R., 2012. Glycosylation of prostate specific antigen and its potential diagnostic applications. Clin. Chim. Acta 413, 1500–1505. https://doi.org/10.1016/j.cca.2012.06.007

West, A., 2018. Chapter 3 - Experimental Methods to Investigate Self-Assembly at Interfaces, in: Ball, V. (Ed.), Interface Science and Technology. Elsevier B.V., pp. 131–241. https://doi.org/10.1016/B978-0-12-801970-2.00003-3

Yan, Q., Zheng, H.-N., Jiang, C., Lia, K., Shou-Jun Xiao, 2015. EDC/NHS activation mechanism of polymethacrylic acid: anhydride versus NHS-ester. RSC Adv. 5, 69939–69947. https://doi.org/10.1039/C5RA13844B

Zeng, Q., 2018. Size matching effect on Wenzel wetting on fractal surfaces. Results Phys. 10, 588–593. https://doi.org/10.1016/j.rinp.2018.07.010

Figure captions

Figure 1. Schematic representation of a lectin-based interdigitated impedimetric-based (IIB) biosensor as a sensing platform for detecting PSA glycan.

Figure 2. Bare Au-IDE. (A) SEM image of the working electrodes surface area (number of pairs (bands) = 52, band width = 10 μm, and band gap = 9 μm) with the Au elements characterized using EDS. (B) 3D images show the uniformity of the fabricated interdigitated electrodes on the glass substrate.

Figure 3. Schematic showing (A) AFM images and (B) water contact angle measurements for the (i) bare Au electrode and (ii) up-to-EDC/NHS-modified electrode, respectively.

Figure 4. High-resolution X-ray photoelectron spectroscopy (XPS) spectra of (A) C 1s, (B) O 1s, (C) N 1s, and (D) S 2p for bare Au and functionalized Au surfaces.

Figure 5. (A) Changes in cyclic voltammogram peaks in response to a) bare Au-IDE, b) 11-MUA/EDC/NHS surface modification, and c) lectin/ethanolamine immobilization. (B) When the target binds to the receptor, the redox reaction of $[Fe(CN)_6]^{3-/4-}$ with the working electrode is hindered. (C) Analytical detection of IIB biosensor in the presence of different concentrations of PSA target (inset figure shows the Randles equivalent circuit). (D) Linear calibration curve for the measured Rct in response to the target PSA in the concentration range of 10 pg/mL – 100 ng/mL.

Figure 6. (A) Specificity study of developed lectin based IIB biosensor towards undiluted human serum spiked with PSA in concentration of 1 ng/mL and 10 ng/mL, respectively. (B) Validation using ELISA assay.

Figure 1

Click here to access/download;Figure(s);Figure 1.pptx

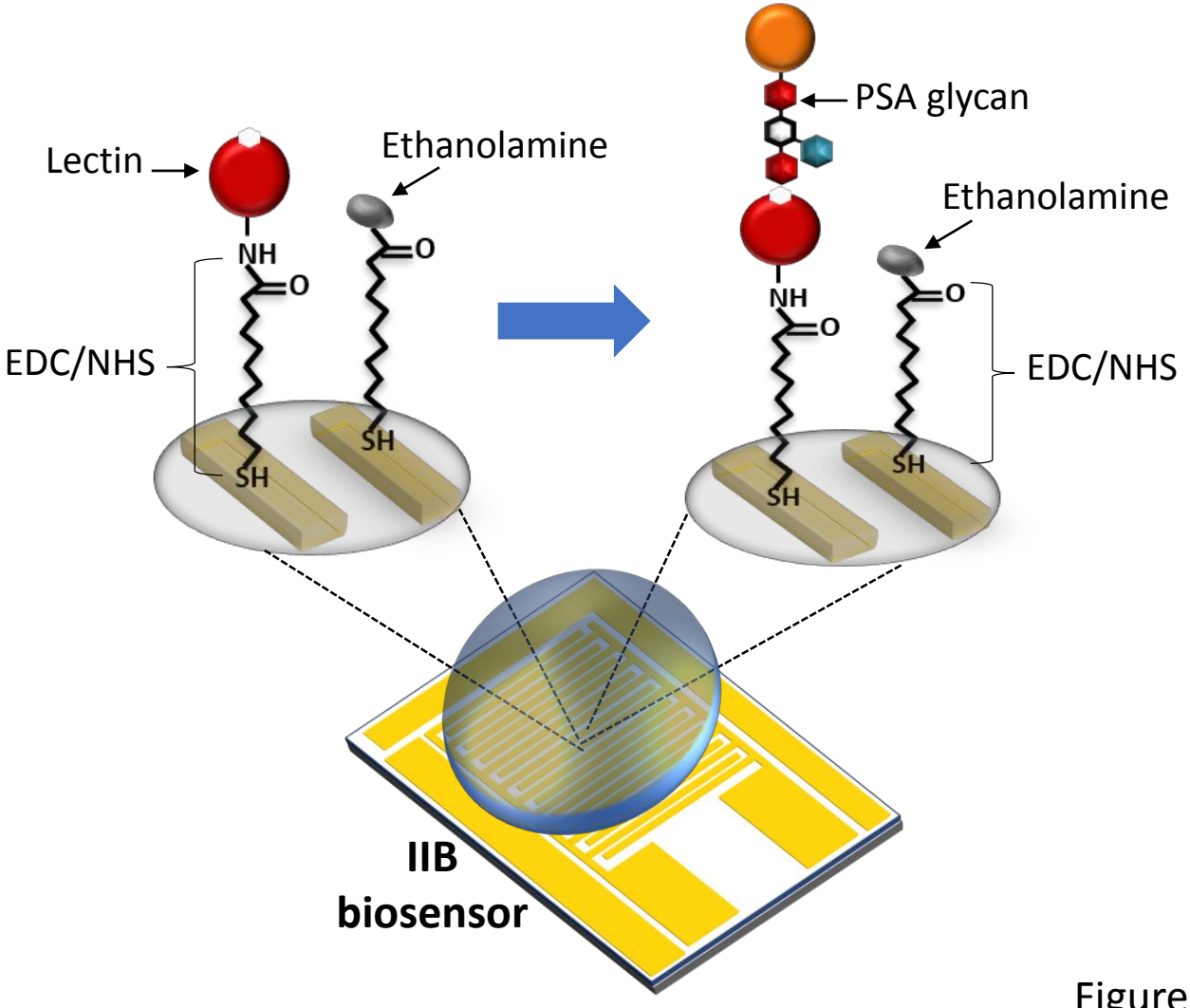

Figure 1

Figure 2

Click here to access/download;Figure(s);Figure 2.pptx

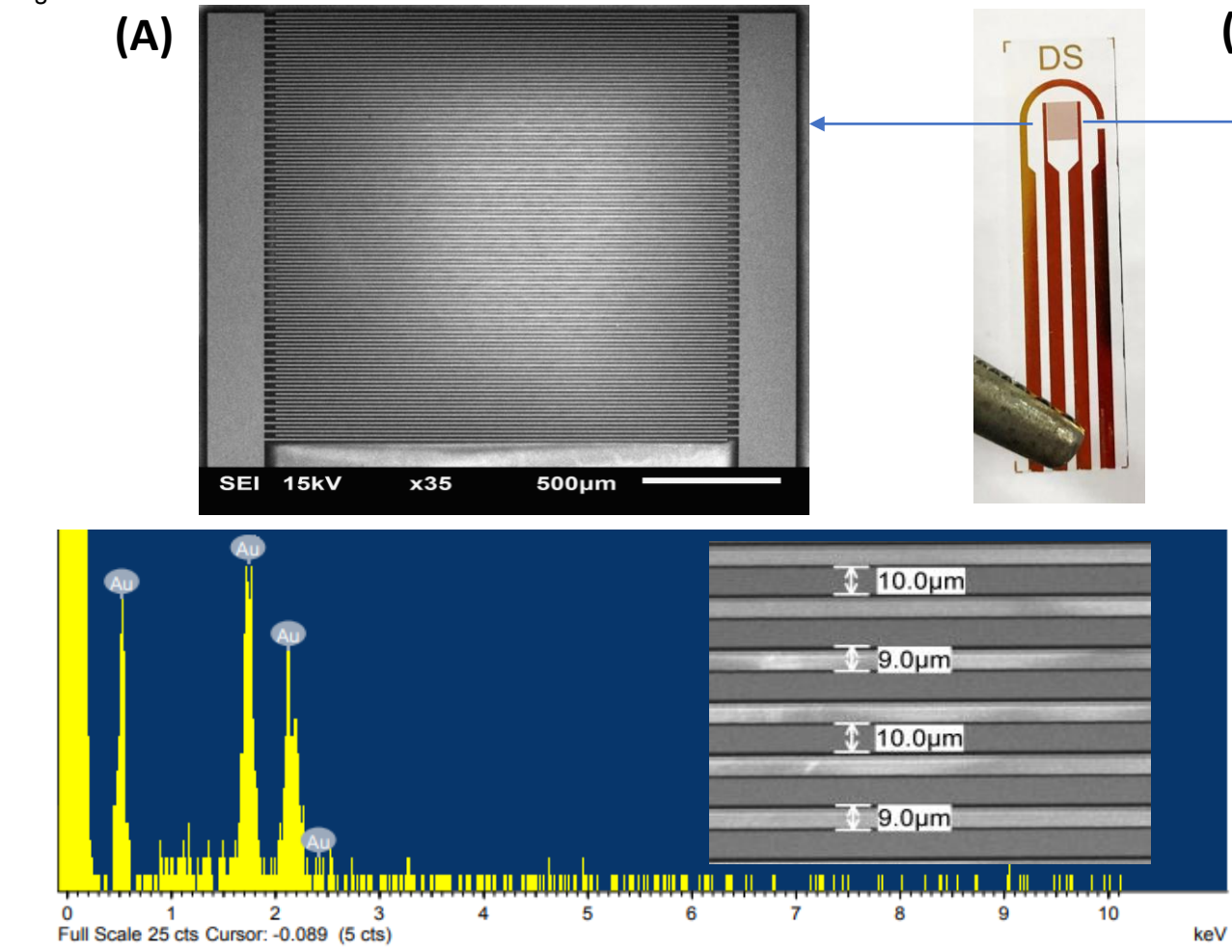

Figure 2

Figure 3

Click here to access/download;Figure(s);Figure 3.pptx

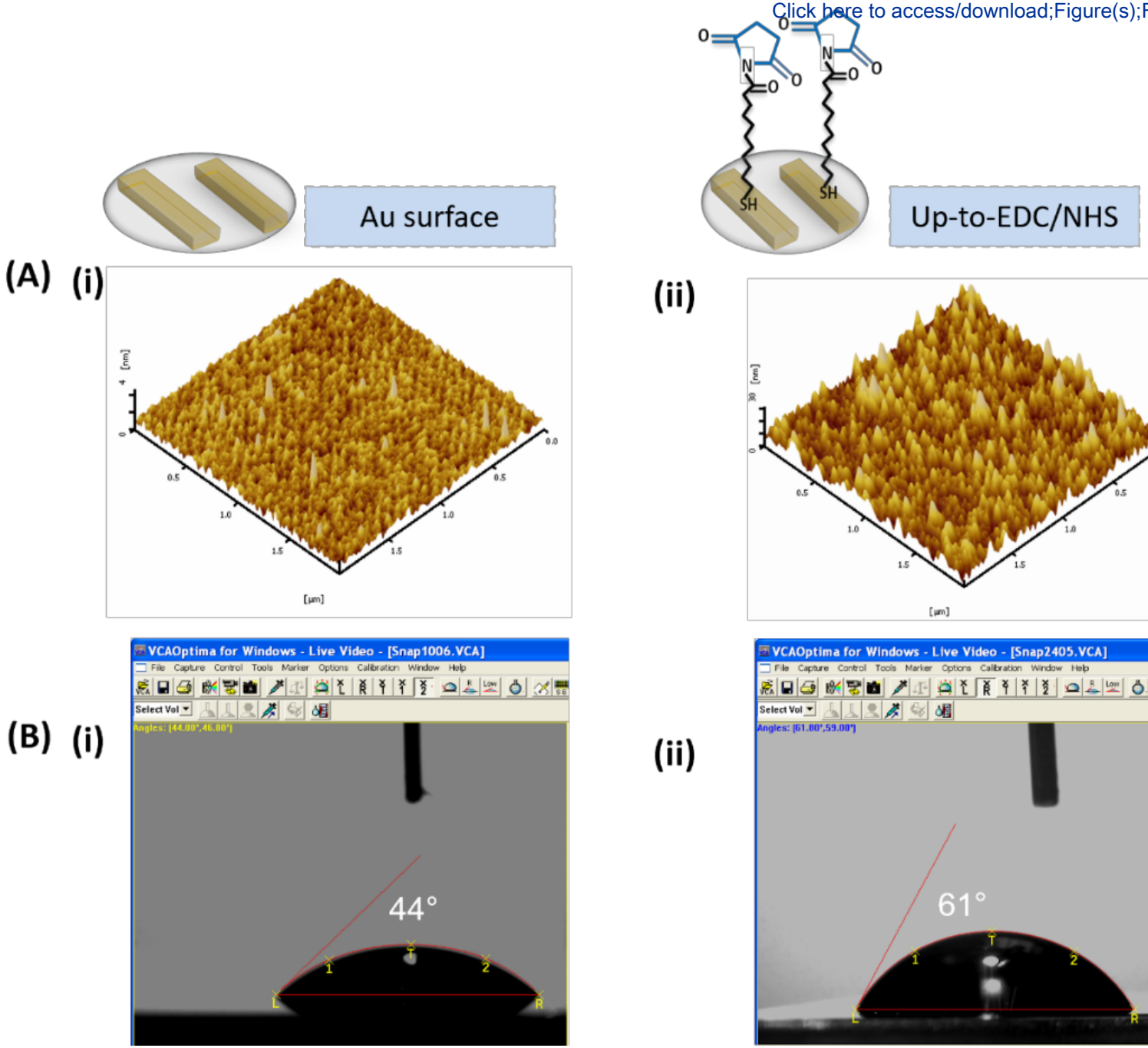

Figure 3

Figure 4

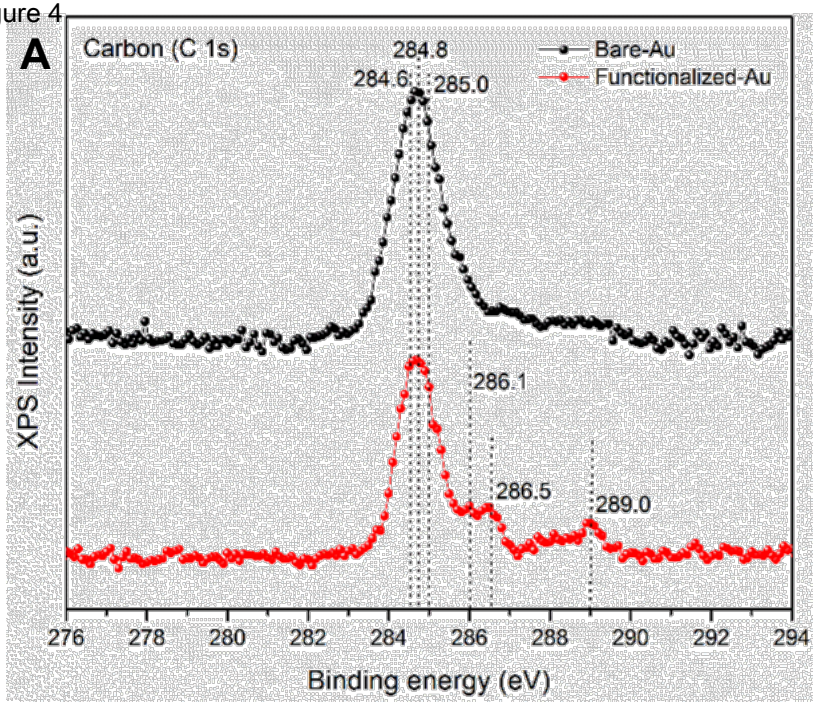

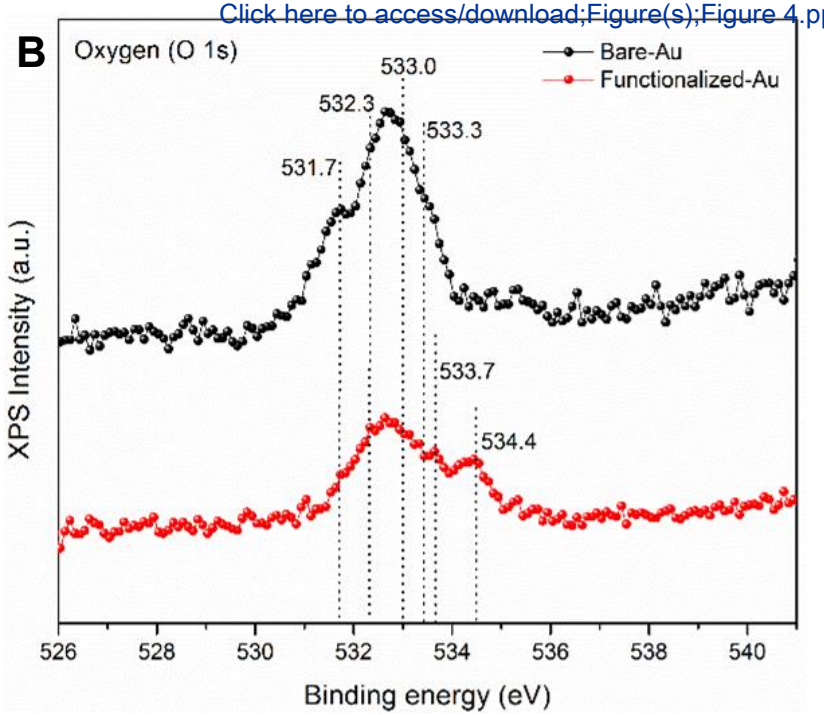

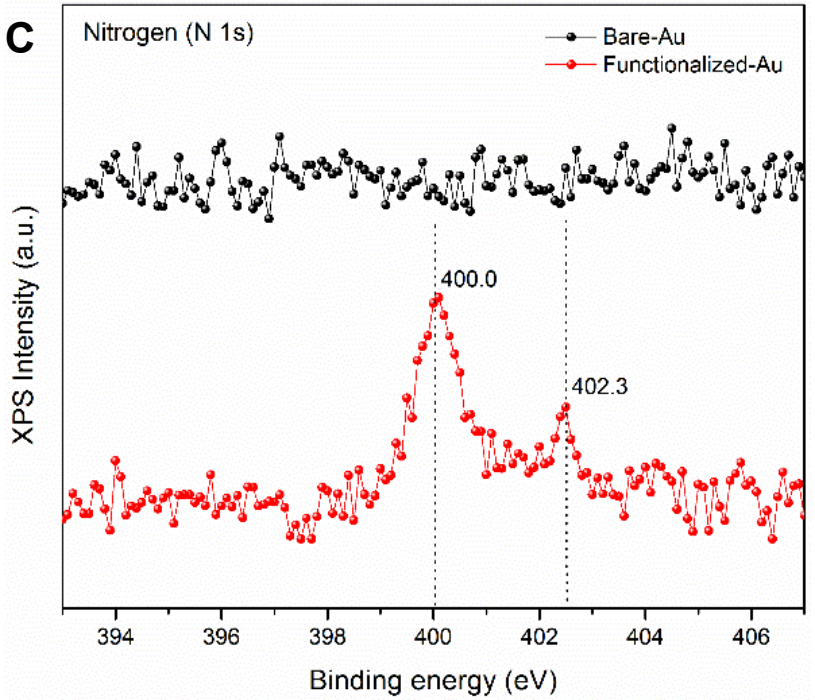

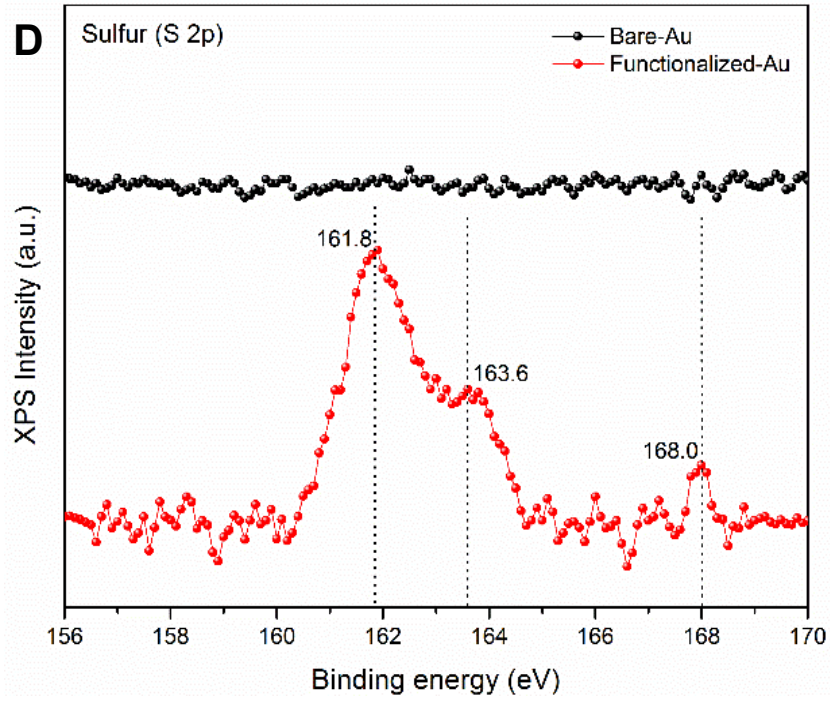

Fig

Figure 5

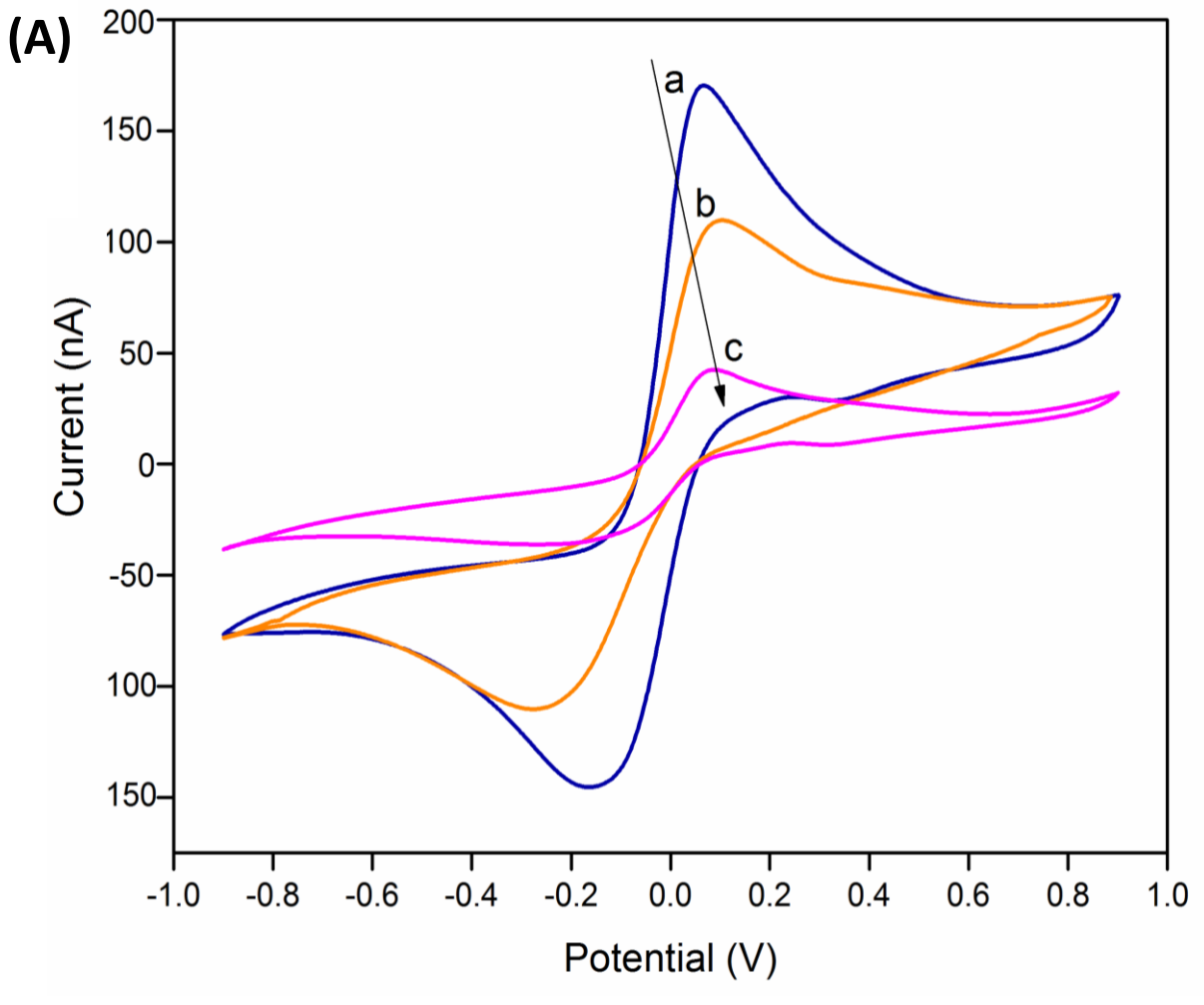

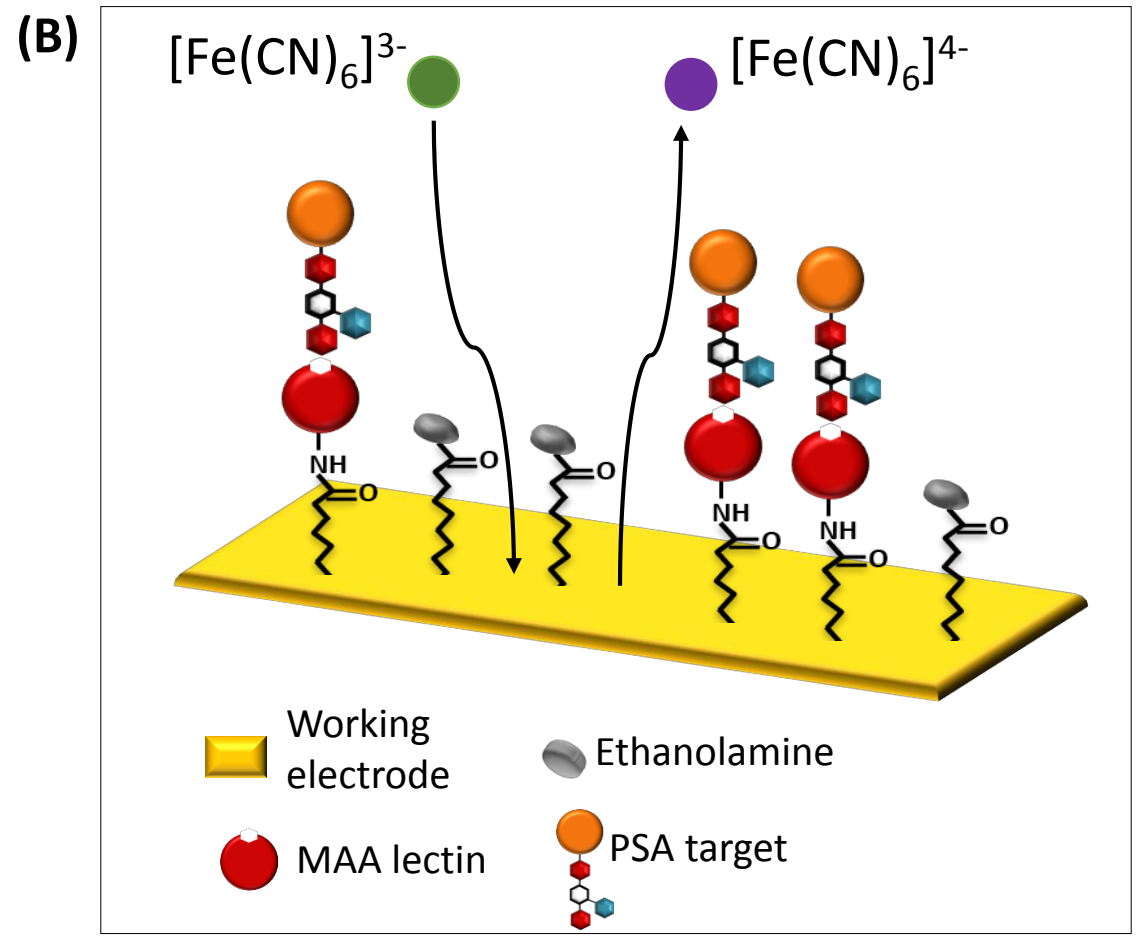

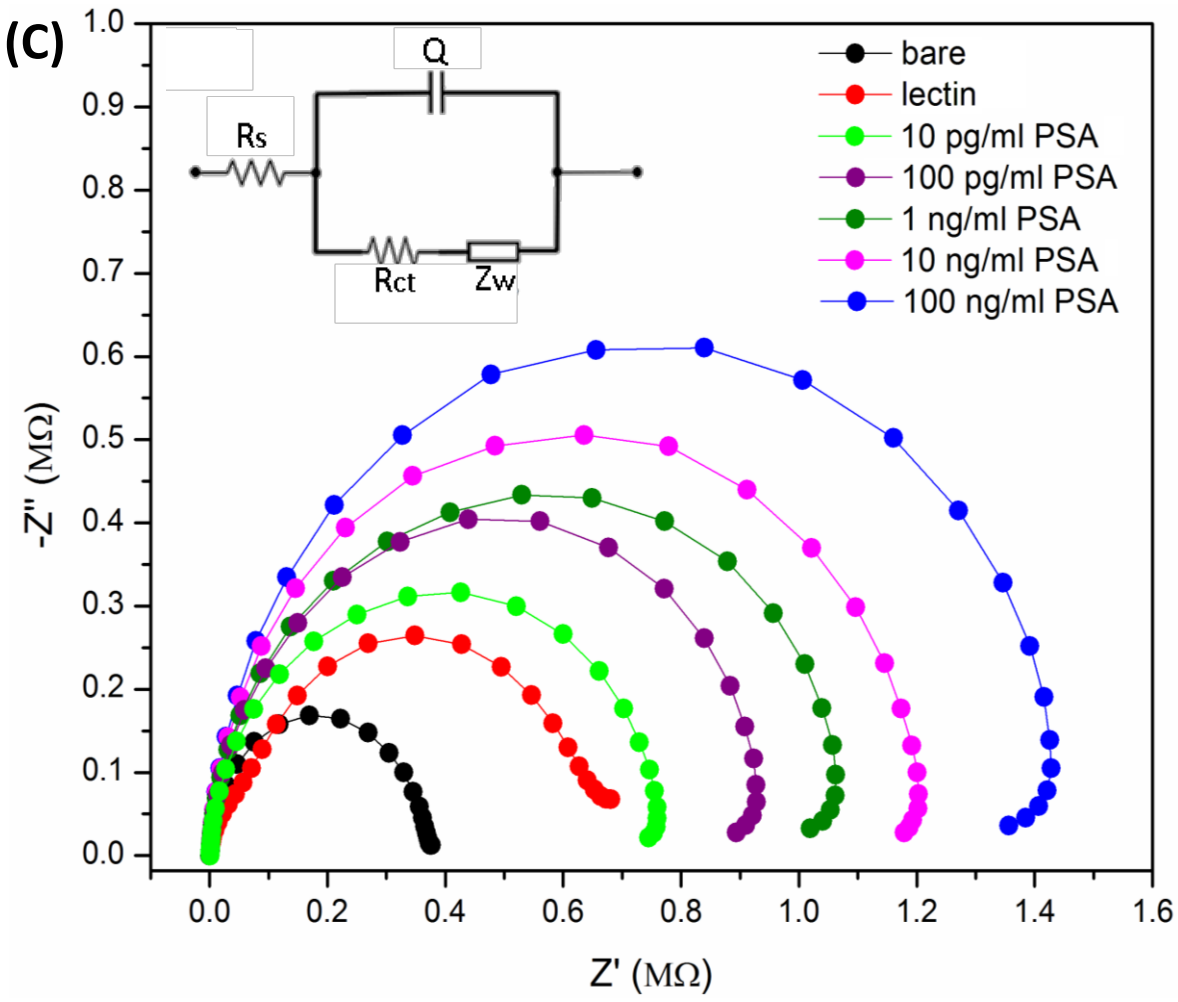

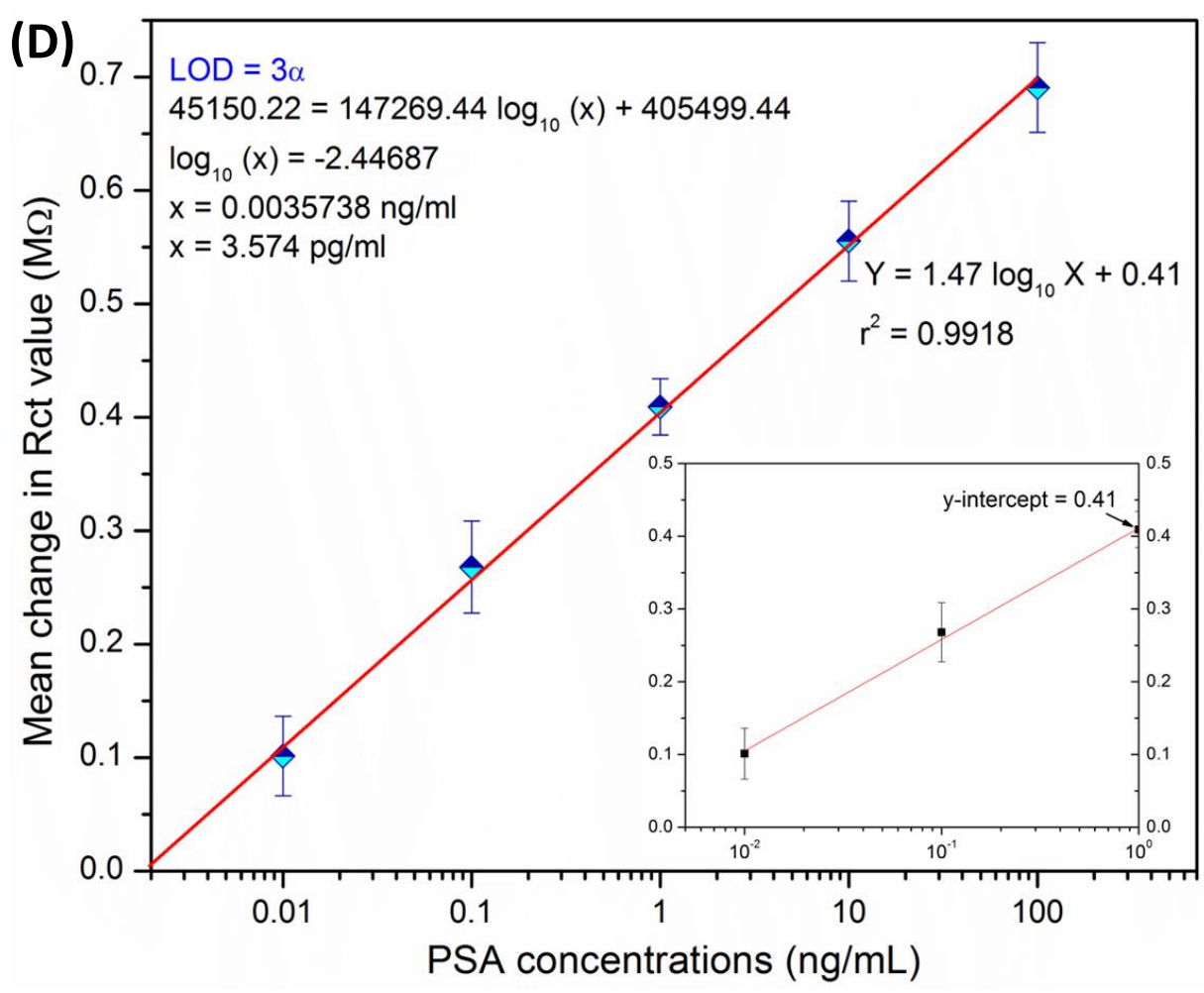

Figure 5

Figure 6

Click here to access/download;Figure(s);Figure 6.pptx

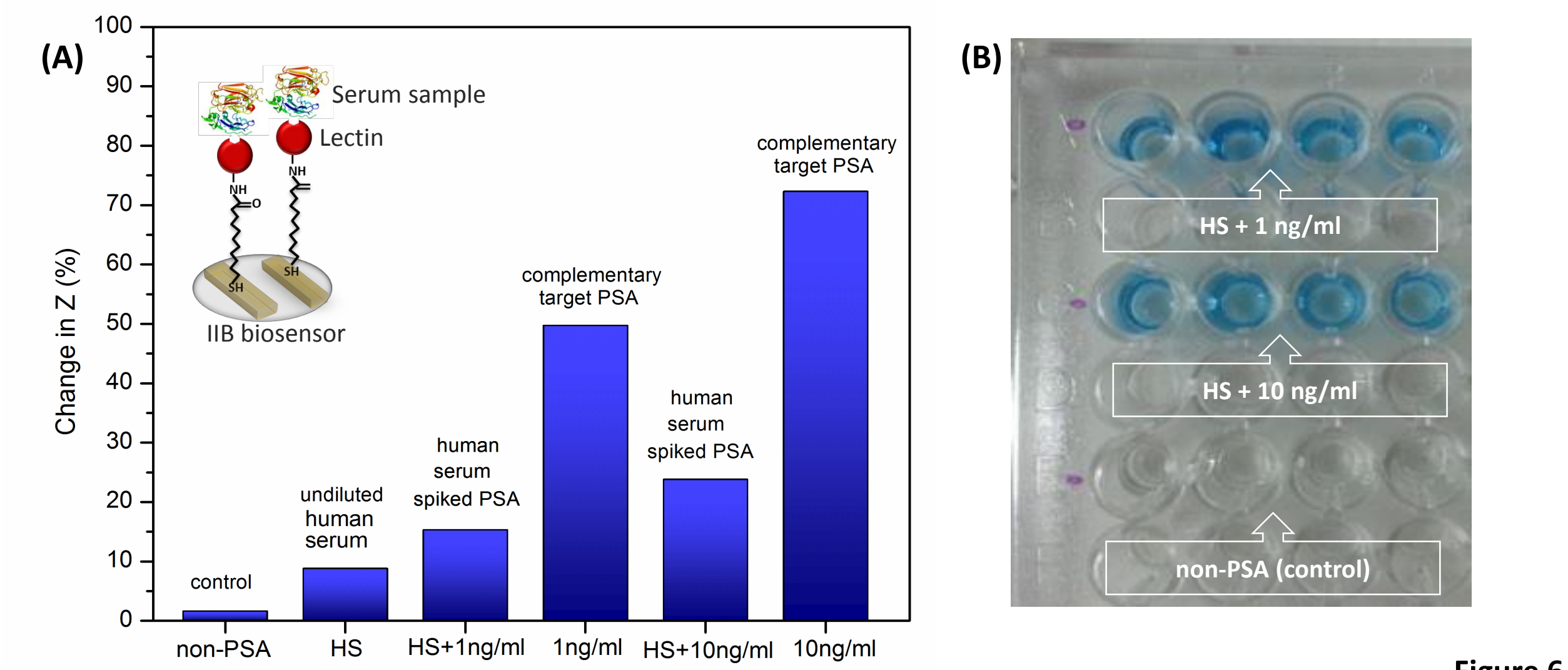

Figure 6